Journal of Hydrology 570 (2019) 598–611

Contents lists available at ScienceDirect

Journal of Hydrology

journal homepage: www.elsevier.com/locate/jhydrol

Research papers

Drywell infiltration and hydraulic properties in heterogeneous soil profiles

Salini Sasidharan[a,b,*], Scott A. Bradford[b], Jiří Šimůnek[a], Stephen R. Kraemer[c]

[a] Department of Environmental Sciences, University of California Riverside, Riverside, CA 92521, USA
[b] United States Department of Agriculture, Agricultural Research Service, U. S. Salinity Laboratory, Riverside, CA 92507, USA
[c] Systems Exposure Division, National Exposure Research Laboratory, Office of Research and Development, US Environmental Protection Agency, Los Angeles, CA, USA

ARTICLE INFO

This manuscript was handled by C. Corradini, Editor-in-Chief, with the assistance of Philip Brunner, Associate Editor

Keywords:
Drywell
Infiltration
Stochastic simulation
Inverse optimization
Effective hydraulic properties
HYDRUS (2D/3D)

ABSTRACT

Drywells are increasingly used to capture stormwater runoff for surface infiltration and aquifer recharge, but little research has examined the role of ubiquitous subsurface heterogeneity in hydraulic properties on drywell performance. Numerical experiments were therefore conducted using the HYDRUS (2D/3D) software to systematically study the influence of subsurface heterogeneity on drywell infiltration. Subsurface heterogeneity was described deterministically by defining soil layers or lenses, or by generating stochastic realizations of soil hydraulic properties with selected variance (σ) and horizontal (X) and vertical (Z) correlation lengths. The infiltration rate increased when a high permeability layer/lens was located at the bottom of the drywell, and had larger vertical and especially horizontal dimensions. Furthermore, the average cumulative infiltration (I) for 100 stochastic realizations of a given subsurface heterogeneity increased with σ and X, but decreased with Z. This indicates that the presence of many highly permeable, laterally extending lenses provides a larger surface area for enhanced infiltration than the presence of isolated, highly permeable lenses. The ability to inversely determine soil hydraulic properties from numerical drywell infiltration results was also investigated. The hydraulic properties and the lateral extension of a highly permeable lens could be accurately determined for certain idealized situations (e.g., simple layered profiles) using constant head tests. However, variability in soil hydraulic properties could not be accurately determined for systems that exhibited more realistic stochastic heterogeneity. In this case, the heterogeneous profile could be replaced with an equivalent homogeneous profile and values of an effective isotropic saturated conductivity (K_s) and the shape parameter in the soil water retention function (α) could be inversely determined. The average value of $K_s$for 100 stochastic realizations showed a similar dependency to I on σ, X, and Z. Whereas, the average value of α had large confidence interval for soil heterogeneity parameters and played a secondary role in drywell infiltration. This research provides valuable insight on the selection of site, design, installation, and long-term performance of a drywell.

1. Introduction

Freshwater resources determine the balance between food security, public health, industrial growth, economic development, environmental sustainability, and the survival of ecosystems across the world (Rosegrant et al., 2002). However, water scarcity occurs in many parts of the world. About 1.1 billion people worldwide lack access to safe water and at least two-thirds of the global population, over 4.0 billion people, live under conditions of severe water scarcity at least 1 month each year (Kummu et al., 2016). Groundwater decline, low or non-existent river flow, and water pollution are some of the major signs of water scarcity (Postel, 2000). Although the global hydrologic cycle produces more freshwater than is needed to sustain the current global population, > 69% of this resource is not available to humans due to rapid runoff or distribution in geographically isolated regions (Postel, 2000). Growing food to meet the needs of the global population requires extraction of a large volume of water and irrigated agriculture accounts for two-thirds of all water withdrawals from natural water resources (Shiklomanov, 2000). The unsustainable pumping of groundwater exceeds the renewable water limits in many regions (Postel, 2000; Postel et al., 1996). Therefore, there is an urgency to find alternative sources of freshwater, to invest in water infrastructure, to develop innovative technologies to recycle, reuse, and preserve stormwater, and to improve water management.

Several countries around the world are practicing artificial or managed aquifer recharge using engineered systems to collect surface water and enhance its infiltration and subsequent movement to aquifers to augment groundwater resources. Infiltration and managed aquifer

* Corresponding author at: USDA, ARS, Salinity Laboratory, Riverside, CA 92507, United States.
E-mail address: salinis@ucr.edu (S. Sasidharan).

https://doi.org/10.1016/j.jhydrol.2018.12.073
Received 20 September 2018; Received in revised form 21 December 2018; Accepted 26 December 2018
Available online 11 January 2019
0022-1694/

recharge can be achieved using surface infiltration (e.g., infiltration basins), direct injection (e.g., aquifer storage, transfer, and recovery), and vadose zone infiltration (e.g., drywells) (Bouwer, 2002; Bouwer et al., 1999; Dillon, 2005; Edwards et al., 2016; Sasidharan et al., 2018) techniques. In recent years, drywells have gained a lot of attention in the United States and across the world. Drywells are vadose zone infiltration wells that end (at least 1–3 m) above the water table (LACDPW, 2014). There are several potential advantages associated with vadose zone infiltration over surface infiltration and direct injection wells. This includes a minimal evaporative loss of water, a small installation area, a large ponding depth, and removal of contaminants in the vadose zone (Edwards et al., 2016; Sasidharan et al., 2018). There are currently > 75,000 drywells in the states of Washington, Oregon, California, and Arizona of the United States (Edwards et al., 2016) and their number is increasing annually. However, not many studies have evaluated the long-term performance of drywells and their environmental impact.

The purpose of a drywell is to transfer water from a poorly drained or low permeable surface capture area to an aquifer for subsurface water storage. The current installation practice involves drilling a drywell at a site and inspecting soil borings or profiles for the presence of layers with adequate permeability to ensure drainage for design storm events (Watt and Marsalek, 2013). However, the lateral extension and vertical continuity of these permeable layers are not determined during well installation. It is logical to anticipate that the position, lateral extension, thickness, and spatial variability of a permeable layer/lens adjacent to a drywell will play a critical role in determining the infiltration behavior. Indeed, an understanding of the soil hydraulic properties has been reported to be a very important factor for the successful design, installation, execution, and long-term performance of a drywell (Edwards et al., 2016). In our previous study, numerical and field-scale experiments were conducted to characterize the drywell infiltration behavior. HYDRUS (2D/3D) computer software was modified to simulate the transient boundary conditions of the Maxwell Type IV drywell geometry. Effective soil hydraulic properties of two drywell sites across California were estimated via inverse optimization of the field-scale falling head data (Sasidharan et al., 2018). However, no studies have systematically investigated the role of subsurface heterogeneity on drywell performance.

Previous studies have attempted to estimate the effective saturated hydraulic conductivity of an unsaturated soil using a constant head borehole test. For example, analytical solutions have been developed to determine the hydraulic properties of a homogenous soil domain using constant head data and numerical simulations have been conducted to evaluate the accuracy of these analytical solutions (Reynolds and Elrick, 1985; Xiang et al., 1997). However, estimates of the hydraulic conductivity were often unrealistic due to the assumption of soil homogeneity in these analytical solutions (Reynolds and Elrick, 1985) and inherent soil heterogeneity. Later, Xiang et al. (1997) proposed an analytical approach to analyze the flow contribution of each layer to the total flow and numerically evaluated the approach and its assumptions. However, this test neglected unsaturated flow and was only suitable for determining the hydraulic conductivity of layered media in thick unsaturated zones. Drywells are used not only to recharge deep groundwater aquifers, but also as a flood control system in paved urban settings where a shallow aquifer may be present. Alternatively, numerical solutions that account for both unsaturated and saturated flow can be used to inversely estimate the unsaturated soil hydraulic parameters of thin as well as thick soil layers/lenses/fractures that are needed to accurately evaluate the performance of a drywell.

The above approaches considered idealized homogeneous or layered soil systems. However, most field soils are highly heterogeneous, and the hydraulic conductivity may change over a short distance. The heterogeneity of a field site can be estimated using ground topography, soil logs, and other geophysical techniques. However, these methods are very expensive and time-consuming and it is unlikely that such detailed information can be obtained for all drywell sites. Alternatively, numerical solutions and stochastic approaches, such as the scaling methodology, can be used to study drywell infiltration. The scaling approach was first introduced by Miller and Miller (1956) who derived scaling relationships between the pressure head and the hydraulic conductivity using the microscopic laws for capillary pressure forces and viscous flow based on the similarity of the pore space (Vereecken et al., 2007). The Miller and Miller (1956) similitude approach has been widely used in the past to analyze flow and transport processes in heterogeneous unsaturated soil systems (Hammel and Roth, 1998; Roth, 1995; Roth and Hammel, 1996; Tseng and Jury, 1994). In the last few decades, several other approaches such as stochastic perturbation methods, the scaleway approach, the stream-tube approach, the aggregation concept, inverse modeling approaches, and data fusion approaches were developed for upscaling of soil water processes (Vereecken et al., 2007). To the best of our knowledge, no published studies have investigated the influence of stochastic vadose zone heterogeneity on the drywell infiltration behavior and the determination of effective unsaturated soil hydraulic properties.

The objective of this study was to investigate the influence of subsurface heterogeneity on drywell infiltration. The HYDRUS (2D/3D) software was used to directly simulate cumulative infiltration volumes for selected drywell geometries and soil heterogeneities under constant or falling head conditions. Subsurface heterogeneity was described in this model deterministically by defining soil layers or lenses, or by generating stochastic realizations of soil hydraulic properties with selected variance and correlation lengths. The numerically generated data were then used in inverse optimizations to determine the hydraulic properties and the lateral extension of individual layers or lenses, or to determine soil hydraulic properties of an equivalent homogeneous profile. The influence of stochastic subsurface heterogeneity parameters (e.g., the variance, horizontal, and vertical correlation length) on cumulative drywell infiltration and equivalent homogeneous profile values of the saturated isotropic hydraulic conductivity (K_s) and the soil water retention function (van Genuchten, 1980) shape factor (α) were determined.

2. Materials and method

2.1. Mathematical model

The HYDRUS (2D/3D) software package (Šimůnek et al., 2018; Šimůnek et al., 2016) was used to simulate drywell infiltration and redistribution in the vadose zone, by numerically solving the 2-dimensional axisymmetric form of Richards equation. The unsaturated soil hydraulic functions were those of van Genuchten (1980) and Mualem (1976). Unless otherwise noted, default values of soil hydraulic parameters (e.g., the saturated soil hydraulic conductivity, K_s; the shape parameter in the soil water retention function, α; the residual soil water content, θ_r; the saturated soil water content, θ_s; the pore-size distribution parameter in the soil water retention function, n; and the tortuosity parameter in the hydraulic conductivity function, l) were taken from the HYDRUS (2D/3D) Soil Catalog (Šimůnek et al., 2011) (Table 1). The van Genuchten hydraulic parameters in the soil catalog of the HYDRUS (2D/3D) software for selected soil textures were taken from (Carsel and Parrish, 1988).

Fig. 1 shows a schematic of an example simulation flow domain, initial conditions, and boundary conditions. This hypothetical 2-dimensional axisymmetrical domain was adapted from the engineering design and the soil log information collected from the Fort Irwin drywell site presented in our previous study (Sasidharan et al., 2018). The initial condition was specified in terms of the soil water pressure head h (x, z) and was set to a constant pressure head of -0.5 m for the entire flow domain. The nodes at the bottom boundary were assigned a free drainage boundary condition. A no-flux boundary condition was assigned to the upper, right, and lower left sides of the flow domain

Table 1
The residual soil water content (θ_r), the saturated soil water content (θ_s), the shape parameter (α), the pore-size distribution parameter (n), the saturated isotropic hydraulic conductivity (K_s) and the tortuosity parameter (l) for different textural classes obtained from the HYDRUS (2D/3D) Soil catalog (Šimůnek et al., 2011).

Soil	θ_r[−]	θ_s[−]	α[m^{-1}]	n[−]	K_s[m min^{-1}]	l[−]
Sandy clay loam (SCL)	0.1	0.39	5.9	1.48	2.18×10^{-4}	0.5
Sandy clay (SC)	0.1	0.38	2.7	1.23	2.0×10^{-5}	0.5
Sand (S)	0.045	0.43	14.5	2.68	4.95×10^{-3}	0.5
Sandy loam (SL)	0.065	0.41	7.5	1.89	7.37×10^{-4}	0.5
Silt loam (SiL)	0.067	0.45	2.0	1.41	7.5×10^{-5}	0.5

(Fig. 1). The complex geometry and the dynamics of water flow in and out of the drywell were implemented as a Reservoir Boundary Condition which is described in detail by Šimůnek et al. (2018) and Sasidharan et al. (2018). The Reservoir Boundary Condition was specified along the left and bottom boundary of the drywell (Fig. 1). Some simulations employed a constant head boundary condition for 200 min at the surface of the drywell or at textural interfaces. Others considered that the drywell was initially filled to its surface, and then allowed for the water level to fall over time to a selected depth as a result of infiltration into the soil profile.

The size of the hypothetical simulation domain was adjusted depending on the considered soil heterogeneity. Simulations that examined the location, lateral extension, thickness of a sandy lens systems (Fig. 2) employed a 3 m wide and 35 m deep domain, the layered system simulations (Figs. 6–8) employed a 5 m wide and 35 m deep domain and 5 m and 20 m wide domains for 1000 and 5000 min simulation (Fig. 8D and E), simulations that examined lateral extension of lenses (Fig. 9) considered a 15 m wide and 50 m deep domain, and stochastic simulations (Figs. 3–5, 10–13) considered a 12 m wide by 40 m deep domain. The simulation domain was discretized into a two-dimensional triangular finite element mesh using the MESHGEN tool available within HYDRUS (2D/3D) (Šejna et al., 2014). The mesh was refined at the left part of the domain where infiltration from the drywell was simulated. To reduce the mass balance error, the finite element mesh was adjusted such that the size of elements was smaller (0.05 m) near the drywell and the grid size was gradually increased with the radial distance from the drywell, with a maximum element size of 0.75 m. In numerical experiments with multiple soil layers (Fig. 8), the finite element mesh was further refined (finite elements between 0.05 and 0.25 m near the drywell) with a maximum element size of 0.75 m to obtain a smaller mass balance error.

2.2. Numerical experiments

2.2.1. Deterministic heterogeneity – Highly permeable lens

Numerical experiments were initially conducted to understand the effects of the position ($Z = -8, -10.5, -20.5$, and -29 m), the lateral extension (width (W) = 0.09, 0.39, 0.89, and 1.9 m and thickness (H) of 0.91 m), and the thickness (H = 0.91, 1.91, 3.91, 5.91 m and W = 0.09 m) of a highly permeable lens (i.e., a sandy lens surrounded by a sandy clay loam soil) on drywell infiltration behavior for 1481 min. A homogeneous (sandy clay loam) flow domain (W = 3 m × H = 35 m) with an inclusion of a sandy lens was considered in these simulations. The two-dimensional (2D) axisymmetrical flow domain, drywell geometry, initial values of the pressure head at the beginning of the simulation, time-variable boundary conditions, and observed (OBS) data (Fig. 2) were adapted from the Fort Irwin drywell falling head experiment presented in Sasidharan et al., (2018). In brief, a fire hydrant was used to flood the detention pond at the Fort Irwin drywell. A pressure transducer connected to a datalogger was lowered into the drywell and the water depth in the drywell was measured every minute for 1481 min. The in-situ soil hydraulic properties ($K_s$and α) were determined by the inverse parameter optimization of the observed falling head data for an equivalent sandy clay loam soil profile using

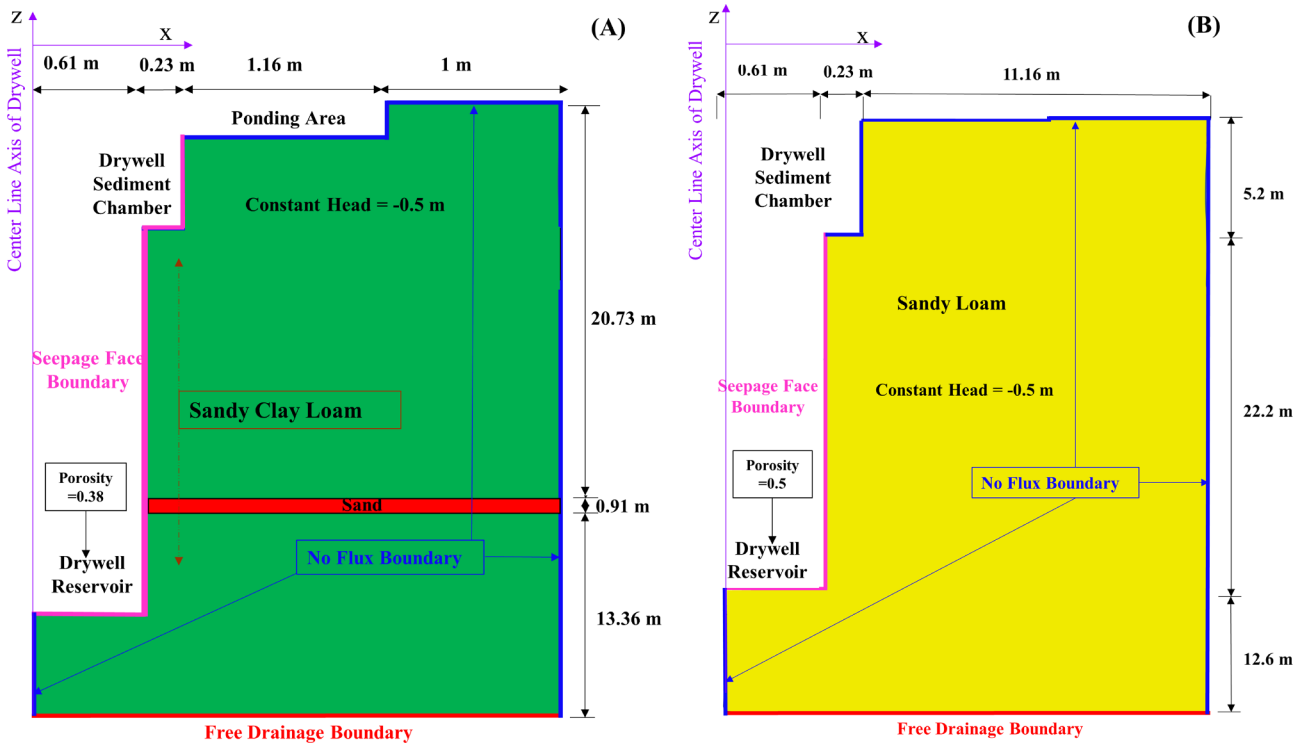

Fig. 1. The geometry, the boundary conditions, and the soil profile for the heterogeneous (sandy clay loam and sand) 2D-axisymmetrical flow domain (with a highly permeable sandy lens) (A) the corresponding results are presented in Fig. 2. The geometry and the boundary conditions for the sandy loam soil profile used in stochastic simulations (B) the corresponding results are presented in Figs. 3, 5, 10, and 11. The corresponding drywell geometry is presented in our previous study (Sasidharan et al., 2018).

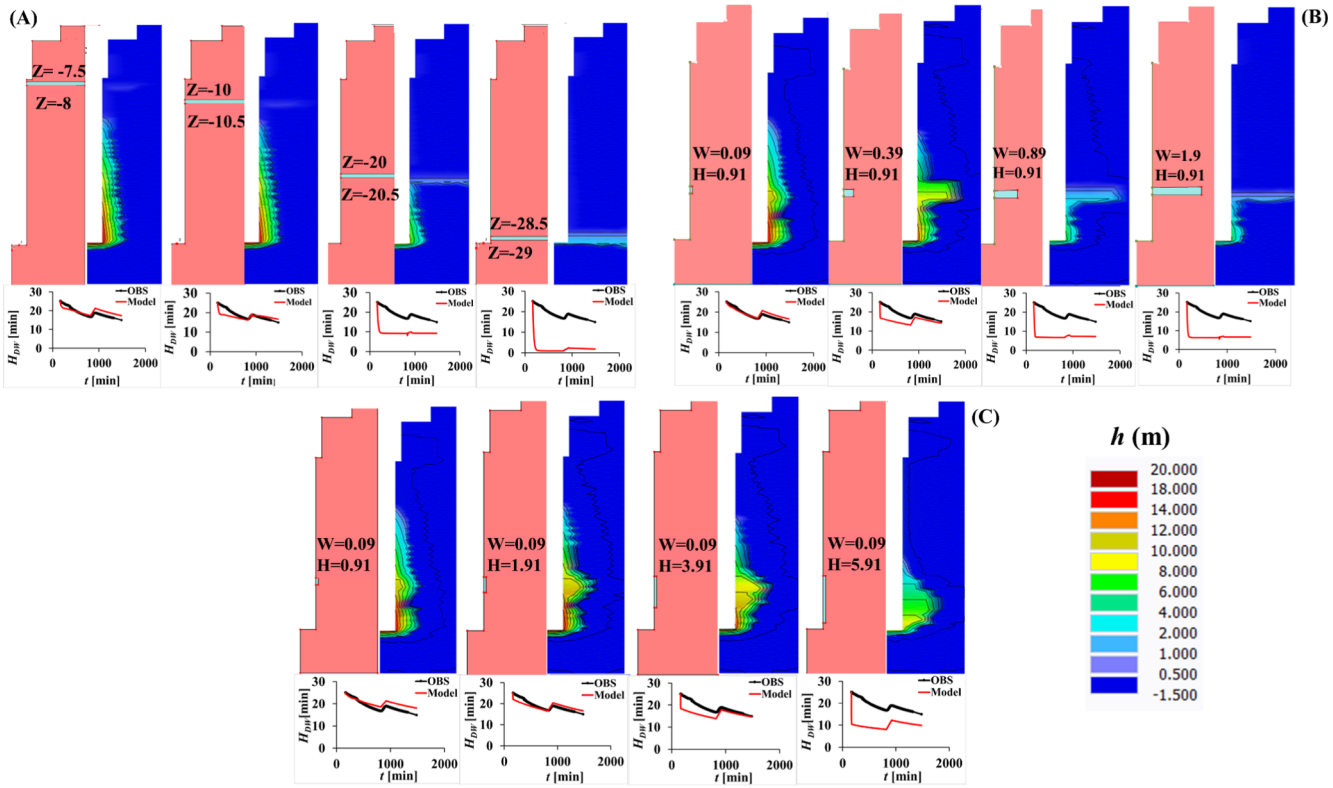

Fig. 2. Flow domains, pressure head profiles (observed data from the falling head experiment at the Fort Irwin drywell (OBS – Black solid line) and simulated data (Model – Red solid line)), and temporal changes in the water level in the drywell (H_{DW}) for continuous sandy lenses at different depths ($Z = -8$, -10.5, -20.5, and -29 m) (A), for sandy lenses with different lateral extensions (W = 0.09, 0.39, 0.89, and 1.9 m), and (B), for sandy lenses with different vertical extensions (thickness) (H = 0.91, 1.91, 3.91, 5.91 m) (C). (For interpretation of the references to color in this figure legend, the reader is referred to the web version of this article.)

HYDRUS (2D/3D) software. The fitted values of K_s and α for sandy clay loam were 2.25×10^{-6} m min^{-1} and 2.63 m^{-1}, respectively, and were employed in this study to be consistent with the drywell at Fort Irwin, CA (Sasidharan et al., 2018).

Additional drywell infiltration experiments (W = 15 m × H = 50 m) were conducted to see if the lateral extension (W = 0, 2.5, 5, 7.5, or 10 m and H = 0.5 m) of the sandy lens in a sandy clay domain could be accurately identified. In this case, a constant head was maintained at the surface of the drywell, and the cumulative infiltration volume (I) and infiltration flux (i) were collected for 5000 min.

2.2.2. Deterministic heterogeneity – Layered soil profile

Numerical experiments were then conducted to determine the effective hydraulic properties of a layered soil profile. A simulation domain of W = 5 m × H = 35 m was used and divided into two or more soil layers. Various layers of the flow domain were assigned different soil hydraulic properties as described in Table 2. Sequential numerical experiments were then conducted to determine infiltration in the layered systems, and to inversely estimate the hydraulic properties from soil layers at the bottom to the top of the drywell using falling (from the drywell inlet to the textural interface) or constant head (200 min at the interface of a soil layer) conditions. The cumulative infiltration volumes (I) from the HYDRUS (2D/3D) direct simulations were determined over time. Values of K_s and α for the bottom soil type were then inversely estimated by fitting to this I data using the parameter estimation procedure in HYDRUS (2D/3D) that is based on the Levenberg-Marquardt nonlinear parameter optimization method (Marquardt, 1963). Table 2 provides a summary of numerical experiments carried out for various two- and multi-layered soil systems, including: the sequence of different soil layers and soil hydraulic parameters used in direct simulations. Direct simulations employed K_s and α values for each soil type from the HYDRUS (2D/3D) Soil Catalog ($K_{sHYDRUS}$ and α_{HYDRUS}, respectively, Table 2). The flow domain was kept the same in both direct and indirect simulations, while the hydraulic parameters for non-fitted layers were kept constant. In falling head experiments, the final pressure head profile after one falling head experiment (half-full well, Fig. 6) was imported as the initial condition for the next simulation (full-well, Fig. 6), and the parameter estimation procedure was repeated for the next layer (Fig. 6). On the other hand, for the constant head simulations, the initial condition was always kept as a constant pressure head of -0.5 m for the entire flow domain for both direct and inverse simulations (Figs. 7 and 8).

2.2.3. Stochastic heterogeneity

The HYDRUS (2D/3D) computer software has an option to generate stochastic (random) distributions of hydraulic conductivity and pressure head scaling factors (α_K and α_h, respectively) using the Miller-Miller similitude approximation (Miller and Miller, 1956). Using this option, a specific K_s value can be assigned to the flow domain (or a part of it) that is then multiplied in each node by a scaling factor α_K. The Miller-Miller scaling procedure requires that $\alpha_K = \alpha_h{}^{-2}$. The stochastic distribution requires three input parameters: the standard deviation (σ) of $\log_{10}(\alpha_K)$, and its correlation length in the lateral (the X-correlation length) and vertical (the Z-correlation length) directions. The value of σ determines the extent of variations in the scaling factors, with higher values leading to higher variations in scaling factors. On the other hand, the correlation length is a measure of the distance in a specific direction that scaling factors are related. A high value of the X-correlation length means that the scaling factor maintains similar values for a greater horizontal distance. The same applies for the Z-correlation length in the vertical direction (Rassam et al., 2003). In this study, the following combinations of the scaling factors with variable σ (σ = 0, 0.25, 0.5,

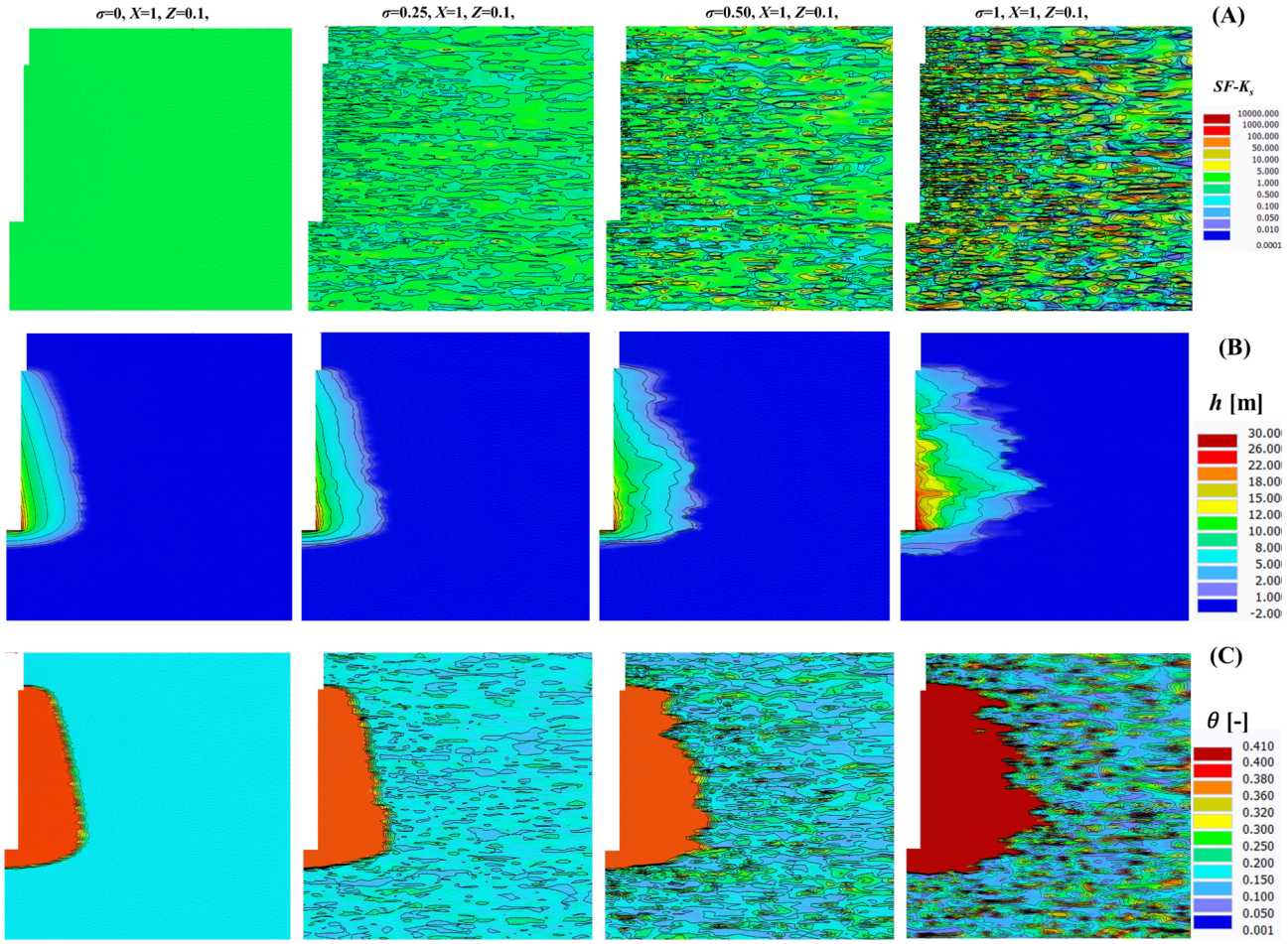

Fig. 3. Heterogeneous sandy loam profiles for the hydraulic conductivity scaling factor (SF-K_s) generated for $\sigma = 0$, 0.25, 0.50, and 1, $X = 1$ m, and $Z = 0.1$ m (A). The corresponding pressure head (h) (B) and soil water content (θ) (C) profiles at 100 min for a constant head experiment.

1;$X = 1$ m; $Z = 0.1$ m), a variable X-correlation length ($\sigma = 1$, with $X = 0.1$, 1, 10 and $Z = 0.1$; and $\sigma = 1$, with$X = 1$, 10 and$Z = 2$), and a variable Z-correlation length ($\sigma = 1$, with $X = 1$ and $Z = 0.1$, 1, 2) were used. Sandy loam was used in the flow domain (W = 12 m × H = 40 m). Forward simulations were conducted for 100 min by maintaining a constant head in the drywell. The I output was collected from each simulation and a total of 100 simulations were done for each combination of stochastic parameters. The mean cumulative infiltration volume (μ_I), 95% Confidence Interval-Upper Limit (95% CI-UL), and 95% Confidence Interval-Lower Limit (95% CI-LL) were calculated.

Accurate determination of soil hydraulic properties of a field site is the key to estimating infiltration from a drywell. A numerical model that can determine the hydraulic properties based on the stratigraphic information of a site can help to identify the best location for the drywell installation. Therefore, the possibility of developing a correlation between the type of the stochastic parameter combination used in the forward simulation, the resultant cumulative infiltration volume, and the effective hydraulic properties of the stochastic field was investigated. Inverse optimization of the I output data obtained from each direct simulation (a total of 100 simulations per a stochastic parameter combination) was conducted. Only the hydraulic parameters K_s andα were optimized while the remaining hydraulic parameters (θ_r, θ_s, n, and l) were kept constant at default values from the HYDRUS (2D/3D) Soil Catalog (Table 1) for sandy loam. IBM Cloud Computing Virtual Servers (IBM, USA) with four computing instances with 48 × 2.00 GHz core and 192 GB RAM were used to perform 800 inverse simulations. Python scripts were used for importing and exporting of input and output data, and for further data analysis. Mean values of K_s, α, 95% CI-UL, and 95% CI-LL were calculated from a total of > 80 inverse simulations.

3. Results and discussion

3.1. A direct (forward) numerical simulations

3.1.1. Deterministic heterogeneity – Highly permeable lens

The current drywell installation practice involves drilling at a potential drywell site until a permeable layer is detected. The permeability of this layer is assumed to infiltrate water efficiently and guarantee the successful performance of the drywell over a specified time duration. Numerical experiments were conducted to investigate the validity of this assumption by simulating drywell infiltration behavior for different high permeability lens locations, lateral extensions, and thicknesses. Fig. 2 presents a comparison of the observed data obtained from the Fort Irwin drywell field scale falling head experiment (Sasidharan et al., 2018) and simulated falling heads for heterogeneous (lenses) domains. Fig. 2A shows the influence of the vertical position of a 50 cm thick continuous sandy lens on the simulated matrix potential (h) profile in the soil adjacent to the drywell after 1481 min, and changes in the drywell head (H_{DW}) over time. The drywell infiltrates water and H_{DW}falls at a faster rate when the sandy lens occurs at a deeper vertical position because of a larger pressure head at the lens boundary. Fig. 2B and C show the effect of a sandy lens's lateral extension and thickness, respectively, on changes in simulated soil matric potential and the drywell H_{DW}over time. Increasing the lateral

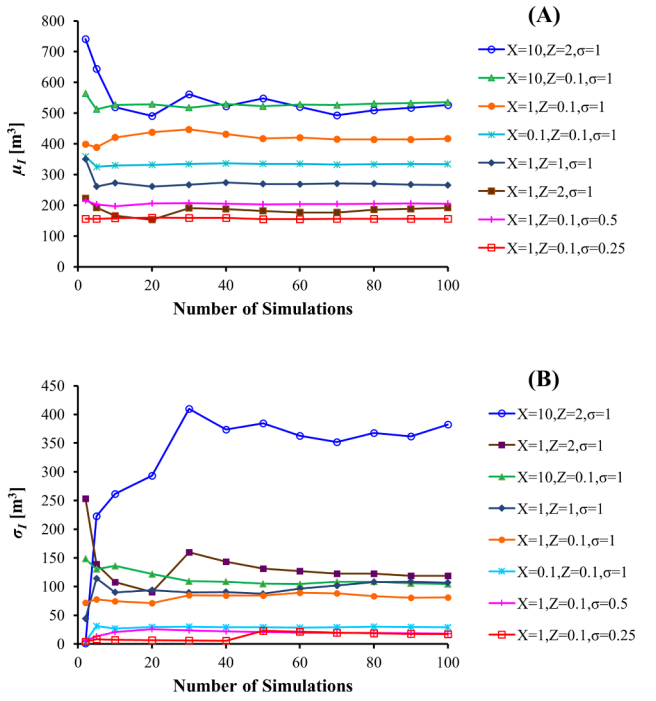

Fig. 4. The mean cumulative infiltration volume (μ_I) (A) and the mean standard deviation of the cumulative infiltration volume (σ_I) (B) as a function of the total number of simulations for all considered combinations of stochastic parameters investigated in this study for a sandy loam flow domain (W = 12, H = 40) for 100 min.

extension and thickness of the sandy lens also increases the water infiltration and the rate of decrease in H_{DW}. The numerical results demonstrated that a highly permeable lens/layer at the bottom of a drywell can infiltrate water at a much faster rate than the same sized lens at the top of a drywell. Furthermore, the cumulative infiltration volume from a drywell increases with an increasing lateral extension and a thickness of a highly permeable lens. However, a thin lateral lens at the bottom of a drywell infiltrated a larger amount of water than an isolated highly permeable lens (a thick, vertically extended lens) due to its greater infiltration surface area. These simulation results clearly indicate that the drywell infiltration performance is sensitive to the high permeability lens location, lateral extension, and thickness. High permeability lens that occurs deeper in the soil profile and has greater lateral and vertical extensions are preferred for infiltration.

3.1.2. Stochastic heterogeneity

The above simulations considered highly idealized scenarios, whereas the natural subsurface is inherently highly heterogeneous. Stochastic simulations were therefore conducted to better understand the effect of random heterogeneities represented by stochastic fields of scaling factors on the cumulative infiltration volume from a drywell. Fig. 3A shows a sandy loam soil profile with increasing heterogeneity from left to right (i.e., σ = 0, 0.25, 0.5, 1; X = 1 m; Z = 0.1 m). The scaling factor for K_s (SF-K_s) shows 8 orders of magnitude variations (0.0001–10000) forσ = 1, which indicates a highly heterogeneous soil profile. Fig. 3B and C show the corresponding h and θ profiles, respectively, at 100 min of simulation for a constant head experiment (a full reservoir). Similar information is presented for the homogeneous domain (σ = 0) as a comparison for results from the heterogeneous domains. The homogeneous wetting front reached a distance of 2.8 m in both horizontal and vertical directions from the bottom of the drywell. In contrast, the wetting front in the heterogeneous profiles extended laterally 3.0, 4.0, and 5.6 m and vertically 2.6, 2.7, and 5.6 m when the value of σ increased to 0.25, 0.50, and 1, respectively.

The same stochastic parameters will produce different realizations of heterogeneity and drywell infiltration behavior. Multiple stochastic realizations were therefore conducted to determine the mean

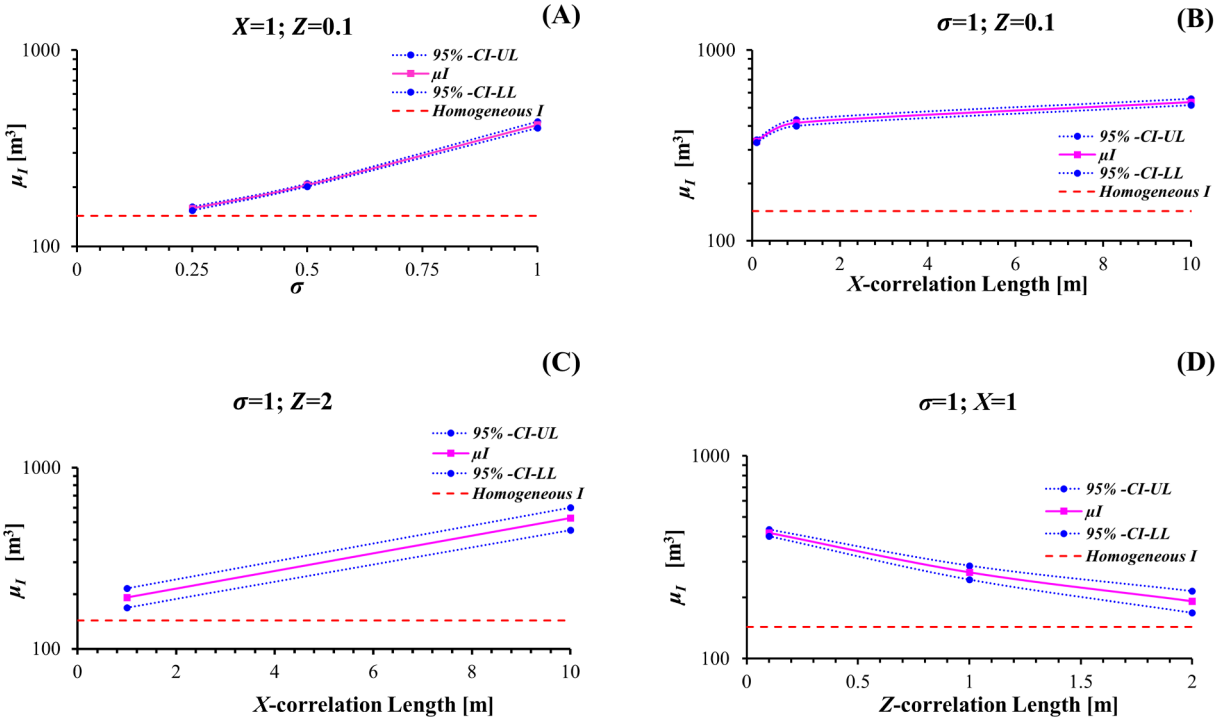

Fig. 5. The mean cumulative infiltration volume (μ_I) (solid line) and the 95% Confidence Interval Upper (95%-CI-UL) and Lower (95%-CI-LL) Limits (dotted lines), as a function of σ (σ = 0.25, 0.5, 1) for X = 1 and Z = 0.1 (A), as a function of X (X = 0.1, 1, 10) for σ = 1 and Z = 0.1 (B), as a function of X (X = 1, 10) for σ = 1 and Z = 2 (C), as a function of Z (Z = 0.1, 1, 2) for σ = 1 and X = 1 (D) for direct stochastic simulations for a sandy loam soil. The *HomogeneousI* (red broken line) value for the homogeneous sandy loam flow domain with K_s and α from the HYDRUS (2D/3D) soil catalog (Table 1). (For interpretation of the references to color in this figure legend, the reader is referred to the web version of this article.)

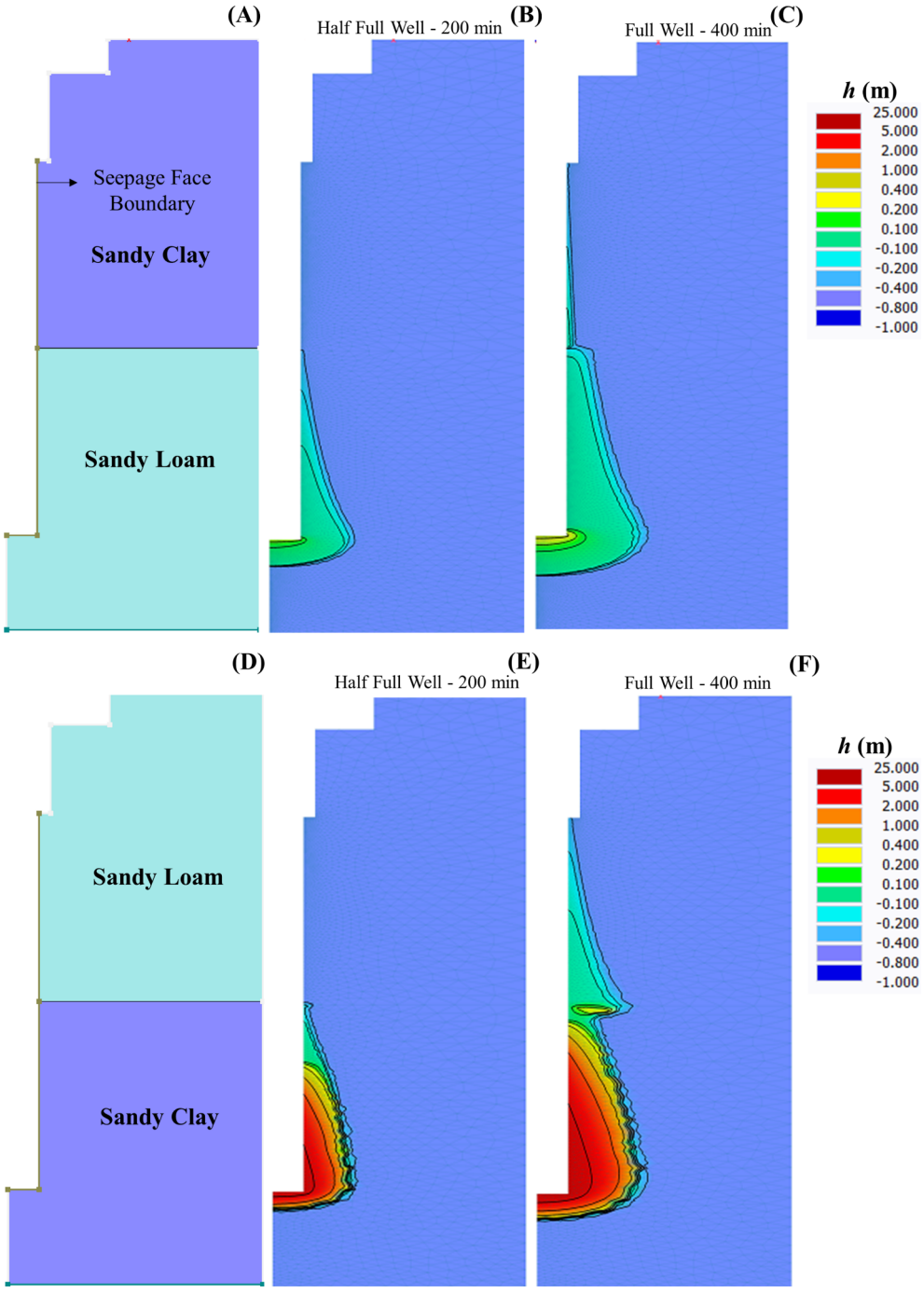

Fig. 6. The two-layered flow domain with sandy clay above sandy loam (SL_B + SC_T) (A) and sandy loam above sandy clay (SC_B + SL_T) (D). The pressure head (h) profiles at 200 min for a half-full well (B, E) and (C, F) 400 min for a full well for falling head experiments. Note that the Reservoir 2 was initially half-full and the water level was then raised at 200 min to the top of Reservoir 2.

cumulative infiltration volume (μ_I) and the mean standard deviation of the cumulative infiltration volume (σ_I). Fig. 4A and B show μ_I and σ_I, respectively, as a function of the total number of simulation realizations for all different combinations of stochastic parameters. The values of μ_I and σ_I stabilize when the total number of simulations was > 75. To be extra conservative, 100 realizations of stochastic heterogeneity parameters were conducted to determine values of $\mu_I$and σ_I in this study. It should be mentioned that the values of $\mu_I$reflect the net effects of the position, lateral extension, and thickness of high permeability lenses. The value of I, μ_I, and its 95% confidence interval as a function of σ (=0.25, 0.5, and 1) when X = 1 and Z = 0.1 m is shown in Fig. 5A. For these stochastic parameters, μ_I increased with σ and exhibited narrow 95% confidence intervals. An increase in σ increases the variability in the K_s scaling factor and leads to the formation of more permeable layers/regions in the soil profile and, consequently, enhanced infiltration from a drywell.

Multiple realizations of drywell infiltration were also conducted for other stochastic parameter combinations. Fig. 5 also presents the calculated values of μ_I and its 95% confidence interval as a function of various X and Z correlation lengths whenσ = 1. Fig. 5B indicates that values of μ_I increased with X and showed narrow 95% confidence intervals when Z = 0.1. The value of μ_I also increased with X when$Z$ = 2 (Fig. 5C), but this increase was more rapid, and the 95% confidence intervals broadened with X in comparison to Fig. 5B. This increase in μ_I

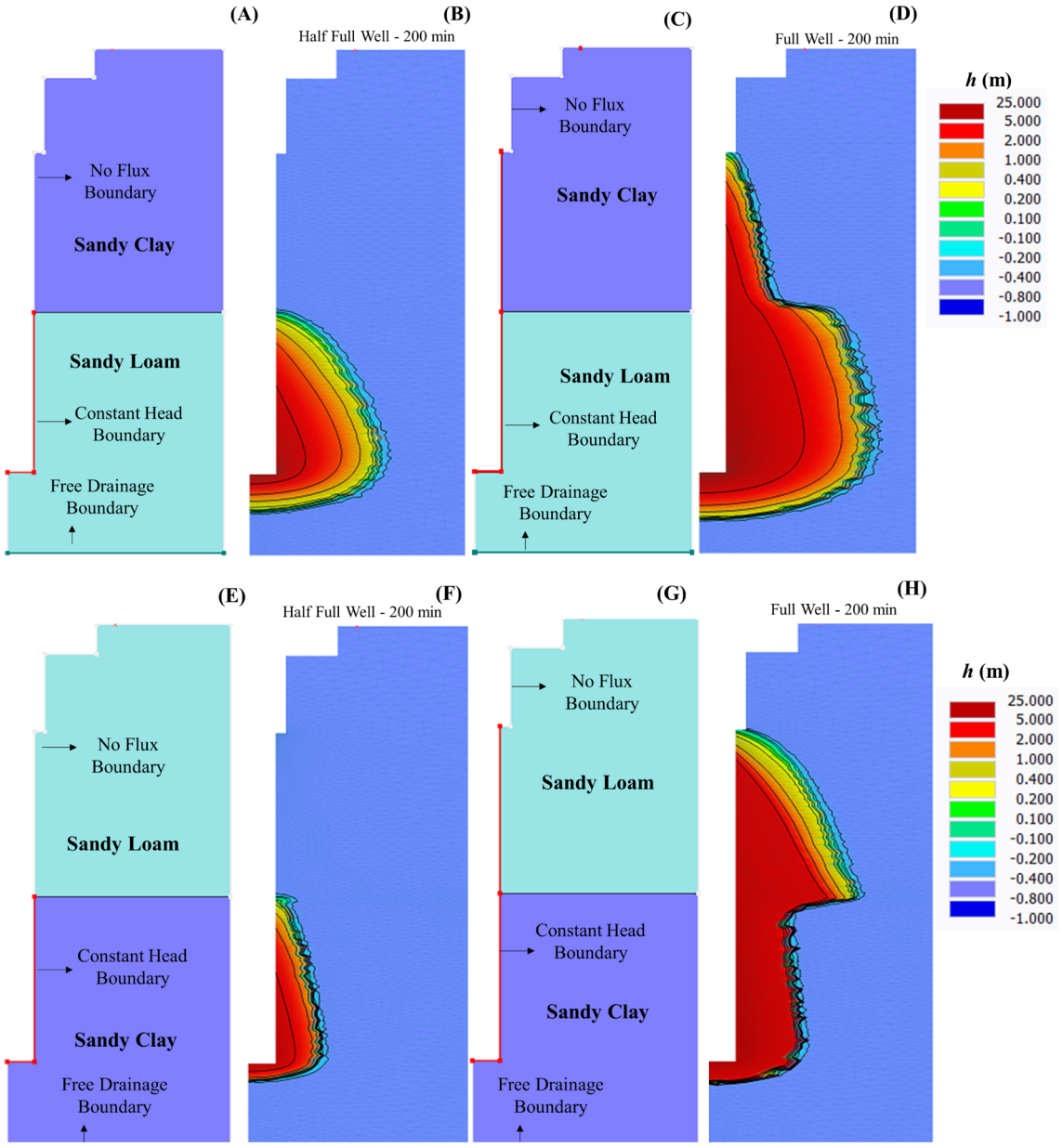

Fig. 7. The two-layered flow domain with sandy clay above sandy loam (SL_B + SC_T) (A, B) and sandy loam above sandy clay (SC_B + SL_T) (E, G). The pressure head (h) profiles at 200 min for constant head BC with a half-full (B, D) and full Reservoir 2 (C, H). The constant head boundary condition is highlighted with a red line. (For interpretation of the references to color in this figure legend, the reader is referred to the web version of this article.)

with X is due to the formation of highly permeable lateral lenses and that enhances the rapid movement of the wetting front in the horizontal direction, and facilities infiltration of water over a larger area. The infiltration area is greater when Z was smaller, and this produced larger values of μ_I (Fig. 5B in comparison to Fig. 5C). Similarly, Fig. 5D shows that μ_I decreased and exhibited very narrow 95% confidence intervals when Z increased. This decrease in μ_I with Z is attributed to the formation of highly permeable isolated lenses and ponded regions with limited infiltration area. The cumulative infiltration volume averaged from 100 stochastic realizations increased with increasing σ and a lateral correlation length, but decreased with an increasing vertical correlation length. Collectively these results indicate that the lateral extent of highly permeable thin layers with a great vertical connectivity enhances rapid infiltration of water from a drywell to the surrounding soil.

3.2. Indirect (Inverse) numerical simulations

Drywell infiltration experiments provide an opportunity to inversely determine equivalent homogeneous hydraulic properties for heterogeneous soil profiles (Sasidharan et al., 2018). Below we numerically investigate the ability to determine soil hydraulic properties of individual layers and lenses, as well as the potential limitations of such an approach in more complex, heterogeneous systems.

3.2.1. Deterministic heterogeneity – Layered soil profile

Table 2 provides a summary of numerical experiments carried out for various two- and multi-layered soil systems, hydraulic parameters, and the statistical parameters for the inverse simulations. Initial simulations considered the effect of a simple two-layered system on drywell infiltration, with a sandy clay layer on the top (SC_T) and a sandy loam layer on the bottom (SL_B), using falling head (from the surface of the drywell to the textural interface) or constant head (water level at the

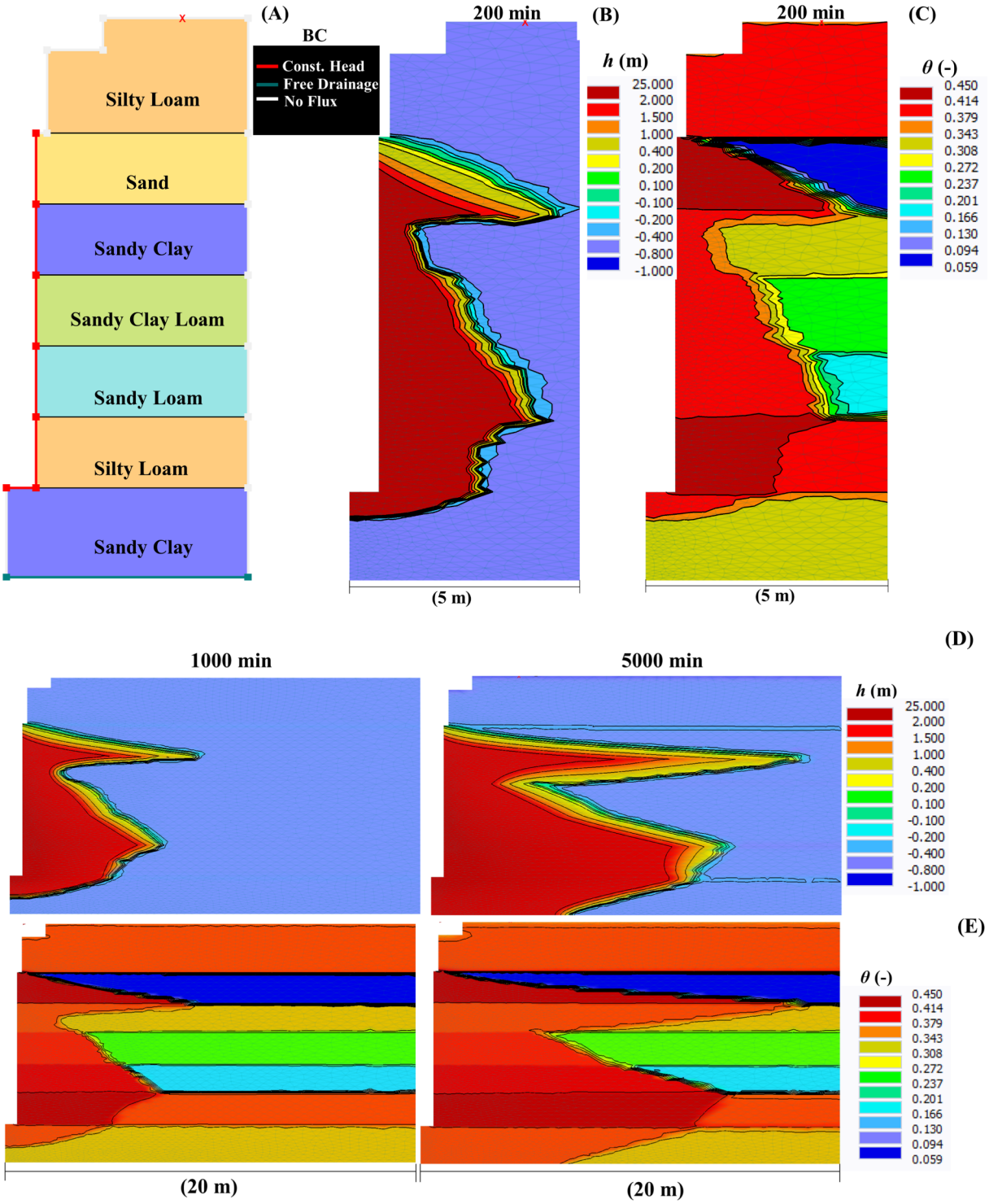

Fig. 8. The flow domain with seven different soil-type layers and boundary conditions (A). The pressure head (h) (B, D) and water content (θ) (C, E) profiles for a constant head boundary (Drywell Reservoir) experiment at 200 min (B, C) and at 1000 and 5000 min (flow domain W = 20 m H = 35 m) (D, E).

textural interface) conditions in the drywell. Similar simulations were also conducted with the soil layers reversed; e.g., sandy loam layer on top (SL_T) and sandy clay layer on the bottom (SC_B). Table 2 indicates that a very good agreement was obtained between the direct and inversely simulated I data with a coefficient of determination (R^2) > 0.99. Furthermore, the fitted values of K_s (K_{sfit}) and $K_{sHYDRUS}$ were always consistent. Similarly, the fitted values ofα (α_{fit}) and α_{HYDRUS} showed good agreement for constant head experiments, but α_{fit} for SL was underpredicted during the SC_T + SL_B experiment with the falling head drywell condition. An explanation for this behavior can be obtained from the simulated profiles of h for these layered simulations (Figs. 6 and 7). A distinct wetting front occurs in both SC and SL layers, as well as between them, during the constant head experiments due to the continuous flow of water (Fig. 7). In contrast, only a relatively small volume of water was available for infiltration during the falling head experiments and this produced a gradual change in the pressure heads of both soil layers, especially when the highly permeable SL was below a less conductive SC layer (Fig. 6).

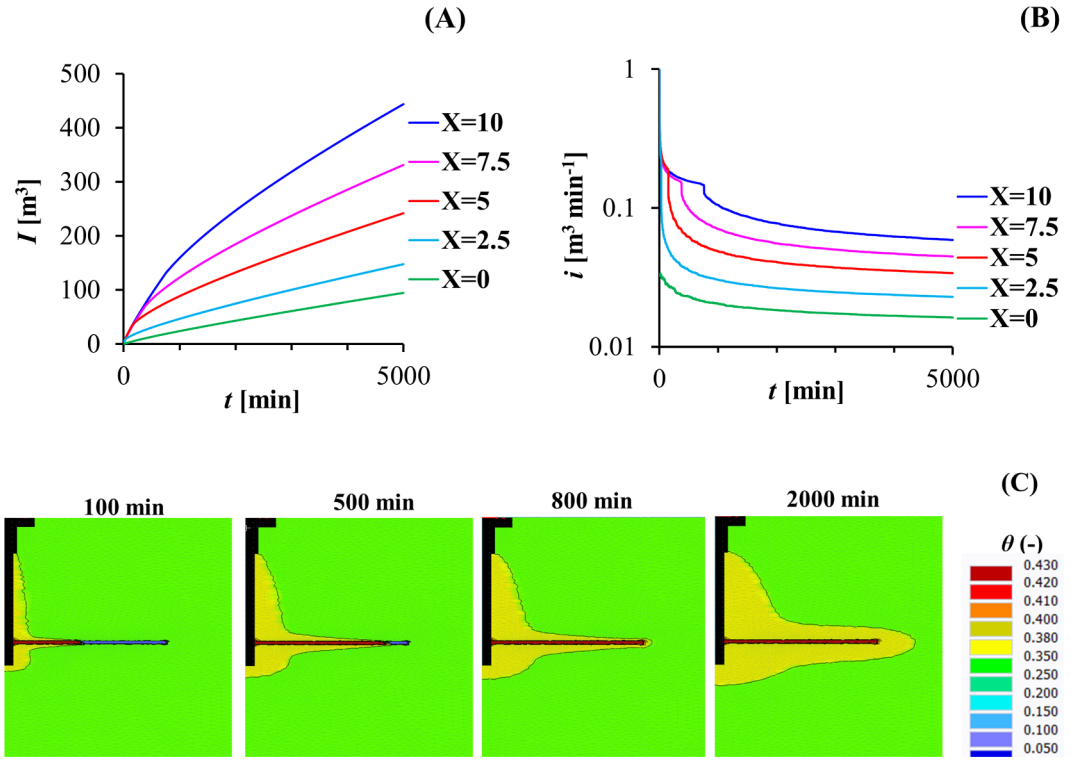

Fig. 9. The cumulative infiltration volume (I) (A) and the infiltration flux (i) (B) for the sandy clay domain with a sandy lens with lateral extensions (X) of 0, 2.5, 5, 7.5, and 10 m and the vertical extension (H) of 0.5 m. Water content profiles for the sandy clay domain with a 0.5 × 10 m sandy lens at 100, 500, 800, and 2000 min for a constant head boundary (Drywell Reservoir) experiment (C).

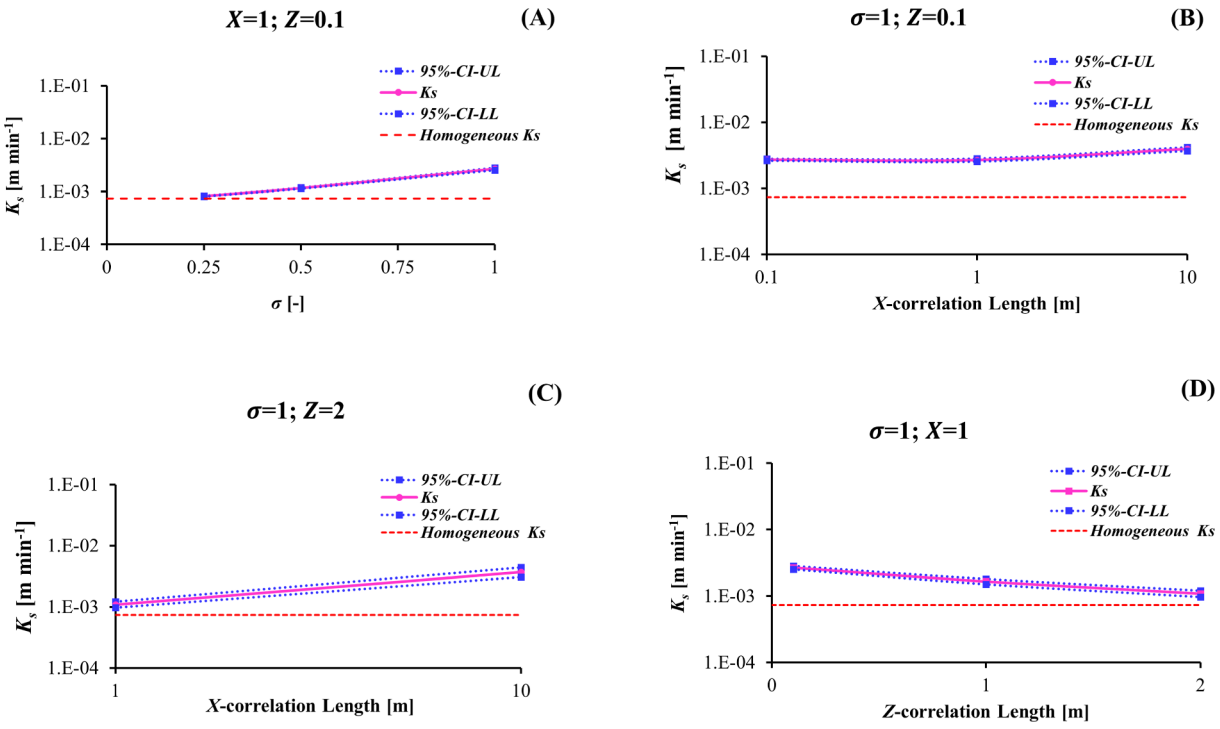

Fig. 10. The mean fitted values of the saturated isotropic hydraulic conductivity(K_s) (solid line) and the 95% Confidence Interval Upper (95%-CI-UL) and Lower (95%-CI-LL) Limits (dotted lines), as a function of σ (σ = 0.25, 0.5, 1) for X = 1 and Z = 0.1 (A), as a function of X (X = 0.1, 1, 10) for σ = 1 and$Z$ = 0.1 (B), as a function of X (X = 1, 10) for σ = 1 and Z = 2 (C), as a function of Z (Z = 0.1, 1, 2) for σ = 1 and X = 1 (D) for inverse stochastic simulations for a sandy loam soil. The *Homogeneous*K_s (red broken line) value for sandy loam soil from the HYDRUS (2D/3D) soil catalog (7.37×10^{-4} m min^{-1}) (Table 1). (For interpretation of the references to color in this figure legend, the reader is referred to the web version of this article.)

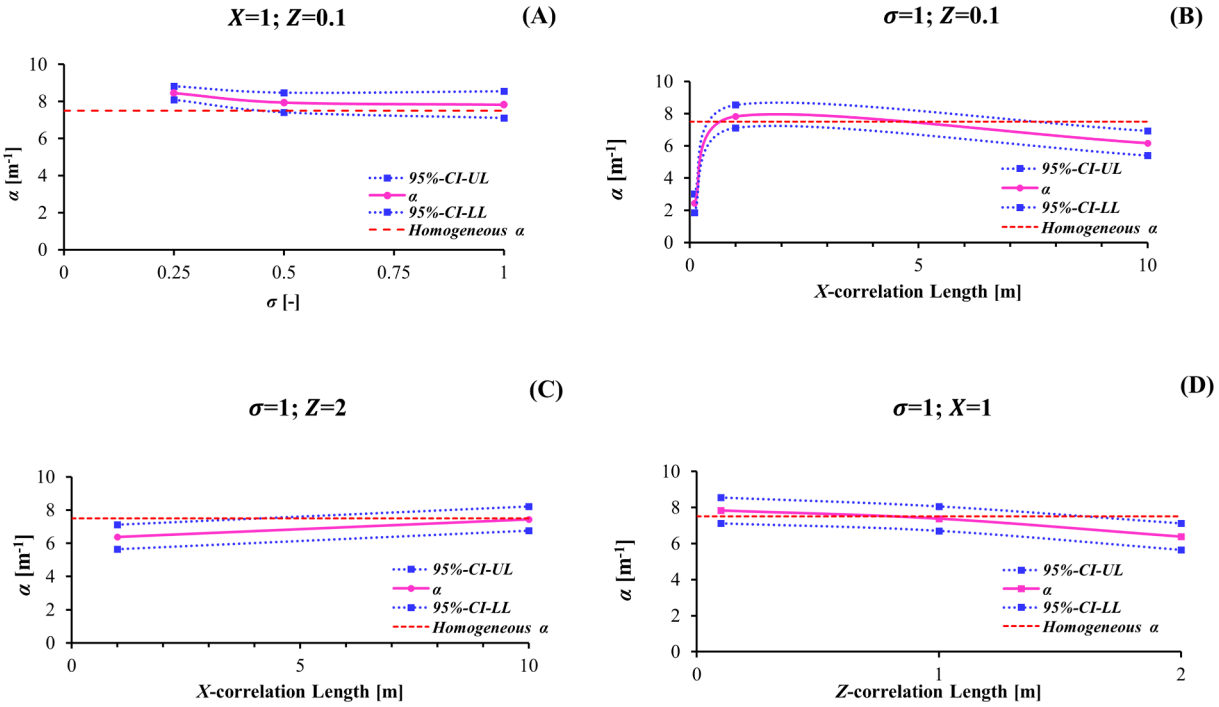

Fig. 11. The mean fitted values of the shape parameter (α) (solid line) and the 95% Confidence Interval Upper (95%-CI-UL) and Lower (95%-CI-LL) Limits (dotted lines), as a function of σ (σ = 0.25, 0.5, 1) for$X$ = 1 and Z = 0.1 (A), as a function of X (X = 0.1, 1, 10) for σ = 1 and Z = 0.1 (B), as a function of X (X = 1, 10) for σ = 1 and Z = 2 (C), as a function of Z (Z = 0.1, 1, 2) forσ = 1 and X = 1 (D) for inverse stochastic simulations for a sandy loam soil. The *Homogeneous*α (red broken line) for sandy loam from the HYDRUS (2D/3D) soil catalog (7.5 m^{-1}) (Table 1). (For interpretation of the references to color in this figure legend, the reader is referred to the web version of this article.)

Additional numerical experiments were conducted to see if hydraulic properties for a soil profile consisting of 7 soil layers could be inversely determined from constant head infiltration studies at the top of each layer. From top to bottom the soil layers are SiL, S, SC, SCL, SL, SiL, and SC (Fig. 8A); where S, SCL, and SiL denote sand, sandy clay loam, and silty loam, respectively. Similar to the two-layered experiments, I data was well described by the model (R^2 > 0.99) and values of K_{sfit} and α_{fit} were consistent with $K_{sHYDRUS}$ and α_{HYDRUS}, respectively. A very distinct pattern in h and θ profiles was observed in Fig. 8B and C, respectively, which reflects the K_s value of each layer (Table 2). For

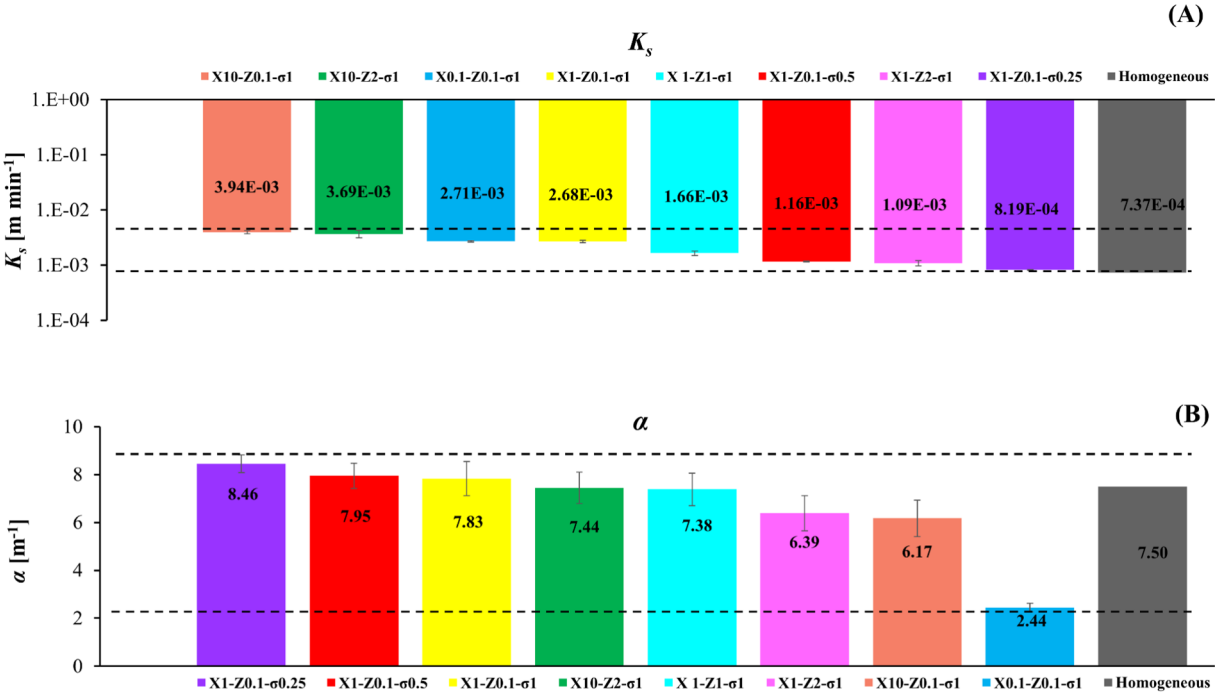

Fig. 12. A comparison of mean fitted values of K_s (A) and α (B) obtained by > 80 inverse optimization of the cumulative infiltration volume collected from eight stochastic realizations of different parameter combinations presented in this study. Also shown are the default K_s and α values of sandy loam from the HYDRUS (2D/3D) soil catalog used in the homogeneous domain.

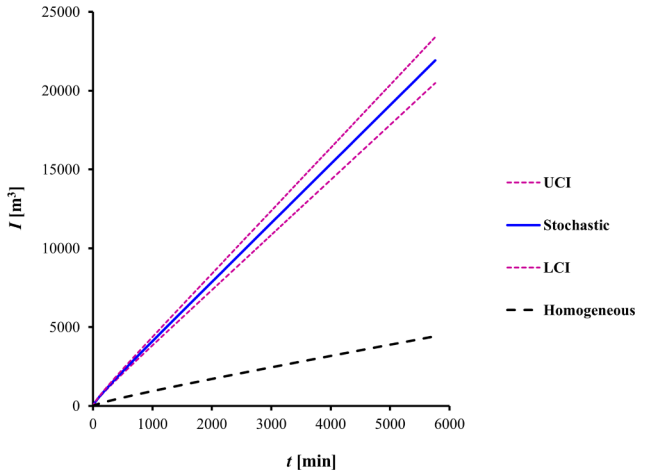

Fig. 13. The cumulative infiltration volume (I) for a homogeneous sandy loam flow domain with K_s and α values obtained from the HYDRUS (2D/3D) soil catalog ($K_s = 7.36 \times 10^{-4}$ m min^{-1} and $\alpha = 7.5$ m^{-1}) (black broken line-Homogeneous), and for a stochastic domain ($X = 10$; $Z = 0.1$; $\sigma = 1$) with inversely optimized parameter values of average $K_s = 3.94 \times 10^{-3}$ m min^{-1} and $\alpha = 6.17$ m^{-1} (blue solid line-Stochastic), Upper-Confidence-Interval (UCI) values of $K_s = 3.68 \times 10^{-3}$ m min^{-1} and $\alpha = 5.40$ m^{-1} (magenta broken line-UCI), and Lower-Confidence-Interval (LCI) values of $K_s = 4.20 \times 10^{-3}$ m min^{-1} and $\alpha = 6.94$ m^{-1} (magenta broken line-UCI). The K_s and α values were presented in Fig. 12. (For interpretation of the references to color in this figure legend, the reader is referred to the web version of this article.)

example, a large lateral extension of the wetting front is apparent in the highly permeable S layer, followed by SL, SCL, SiL, and SC. Note, however, that the lateral extension of the wetting front in a specific layer is also affected by its location in the profile and neighboring two soil layers. For example, when the sand ($K_s = 4.95 \times 10^{-3}$ m min^{-1}) layer is on top of the SC layer ($K_s = 2.0 \times 10^{-5}$ m min^{-1}), water extents laterally in the SC layer despite of its low permeability. The interface between the SC and S layers provides a large infiltration area for the sandy layer. On the other hand, when the SCL ($K_s = 2.18 \times 10^{-4}$ m min^{-1}) layer is present on top of the SL ($K_s = 7.37 \times 10^{-4}$ m min^{-1}) layer, which has a similar permeability, the two layers facilitates the vertical movement of water over time (Fig. 8D and E). In contrast to Fig. 2, these results demonstrate that the presence of a high permeable layer in a more heterogeneous soil profile has a complex influence on the drywell infiltration capacity which depends on its location and the hydraulic properties of the neighboring layers.

Several field-scale approaches have been developed to determine soil hydraulic properties of boreholes. The atmospheric pressure wave test measures the bulk air permeability of the vadose zone sediments as a function of time lag and subsurface pressure attenuation between the surface and subsurface (Weeks, 1978). However, this method only provides information about the vertical permeability rather than the horizontal permeability and is not suitable for soil with a high moisture content or near-surface soil layers (Weeks, 1978). Similarly, gamma and neutron logs of boreholes only provide information on the vertical distribution of soil stratigraphy and water-filled porosity (Hodges et al., 2012). Xiang et al. (1997) presented a multistep (constant head) permeameter test to determine K_s value for a layered soil using the LAYERK model. LAYERK is an analytic code that was designed to determine the field-saturated hydraulic conductivity and the matric flux potential for individual layers using input parameters including layer thickness, the water level in the borehole, the radius of the borehole, and flow rate. However, this approach is only suitable for estimating the K_s value for thick unsaturated zones where the ratio of the water depth (H) and the borehole radius (a) was $\frac{H}{a} \geq 20$ (Jain et al., 2006; Xiang and Chen, 1993; Xiang et al., 1997). In contrast, a drywell's $\frac{H}{a}$ value can range from approximately 10 to 60. Also, in the absence of an independent determination of α, there are some doubts about the practicality of using borehole permeameter test to measure K_s (Archer et al., 2014; Philip, 1985). Moreover, drilling of an additional borehole to perform the above techniques might not be practical at every drywell site because they are expensive, energy intensive, time-consuming, require a dry drilling method (a difficult technique), and need vast expertise. On the other hand, the presented numerical modeling approach using HYDRUS (2D/3D) software can be used to successfully design experimental methodologies to determine effective soil hydraulic properties of a field site regardless of the depth and radius of a drywell. However, we acknowledge that validation of the model using site specific infiltration experiment is essential but goes beyond the scope of this study.

3.2.2. *Deterministic heterogeneity – Highly permeable lens*

The infiltration capacity of a drywell is not only determined by the presence of a highly permeable lens but also by its lateral extent (Fig. 2). However, the inverse optimization technique discussed above only considered layered soil profiles surrounding the drywell, but not

Table 2
The summary of various numerical experiments with different positions of soil layers (SL – Sandy loam, SC – Sandy clay, SiL – Silt loam, SCL – Sandy clay loam, S – Sand; subscript B and T for bottom and top, respectively). The saturated isotropic hydraulic conductivity (K_s) from the HYDRUS (2D/3D) Soil Catalog ($K_{sHYDRUS}$) and fitted (K_{sfit}), the standard or coefficient of K_s(SE_{K_s}), the shape parameter α from the HYDRUS (2D/3D) Soil Catalog (α_{HYDRUS}) and fitted (α_{fit}), the standard error coefficient of α (SE_α), the coefficient of determination between the direct simulated and inversely optimized cumulative infiltration volume data (R^2), and the mass balance error (*M. B. Err*).

Experiment	Soil layers	Soil [−]	$K_{sHYDRUS}$ [m min^{-1}]	K_{sfit} [m min^{-1}]	SE_{K_s} [−]	α_{HYDRUS} [m^{-1}]	α_{fit} [m^{-1}]	SE_α [−]	R^2 [−]	M. B. Err [%]
I (falling head experiments)	$SL_B + SC_T$	SL	7.37×10^{-4}	7.37×10^{-4}	9.71×10^{-8}	7.5	7.49	4.92×10^{-3}	1	0.15
		SC	2.0×10^{-5}	1.91×10^{-5}	2.90×10^{-7}	2.7	2.67	3.38×10^{-2}	0.99	0.86
	$SC_B + SL_T$	SC	2.0×10^{-5}	2.01×10^{-5}	1.63×10^{-8}	2.7	2.70	2.70×10^{-3}	0.99	0.0037
		SL	7.37×10^{-4}	7.10×10^{-4}	7.43×10^{-6}	7.5	5.33	7.43×10^{-2}	0.99	0.02
II (constant head experiments)	$SL_B + SC_T$	SL	7.37×10^{-4}	7.37×10^{-4}	4.75×10^{-7}	7.5	7.47	5.28×10^{-2}	1	0.007
		SC	2.0×10^{-5}	1.98×10^{-5}	2.39×10^{-7}	2.7	2.71	7.51×10^{-2}	1	0.01
	$SC_B + SL_T$	SC	2.0×10^{-5}	2.00×10^{-5}	3.65×10^{-8}	2.7	2.70	2.40×10^{-2}	1	0.0071
		SL	7.37×10^{-4}	7.37×10^{-4}	8.90×10^{-7}	7.5	7.51	8.99×10^{-2}	1	0.0099
III (constant head experiments)	SiL_B	SiL	7.50×10^{-5}	7.50×10^{-5}	4.36×10^{-8}	2.0	2.0	8.0×10^{-3}	0.99	0.11
	$SiL_B + SL_T$	SL	7.37×10^{-4}	7.37×10^{-4}	6.64×10^{-7}	7.5	7.46	0.11	0.99	0.03
	$SiL_B + SL + SCL_T$	SCL	2.18×10^{-4}	2.33×10^{-4}	1.12×10^{-6}	5.9	6.66	0.22	0.99	0.02
	$SiL_B + SL + SCL + SC_T$	SC	2.0×10^{-5}	1.33×10^{-4}	4.85×10^{-7}	2.7	1.32	0.06	0.99	0.02
	$SiL_B + SL + SCL + SC + S_T$	S	4.95×10^{-3}	4.43×10^{-3}	6.07×10^{-6}	14.5	14.43	0.48	1	0.03

the lateral extension of a lens. Additional, numerical experiments were therefore conducted to investigate the ability to identify the lateral extension of a sandy lens that embedded in a sandy clay domain. These simulations considered a constant head boundary condition in the drywell reservoir and different horizontal extensions (0, 2.5, 5, 7.5, and 10 m) of a 0.5 m thick sandy lens. Fig. 9A and B show the cumulative infiltration volumes (I) and infiltration rates (i) as a function of time in these simulations. Note that I increases with the length of the sandy lens in Fig. 9A. The value of i also decreases precipitously when the sandy lens gets fully saturated (Fig. 9B). For example, Fig. 9C (at 800 min) shows the θ distribution after 800 min when the lateral extension of the sandy layer is 10 m. In this case, the sandy lens has become completely saturated (at ~761 min), while the corresponding infiltration rate (blue line) in Fig. 9B shows a sudden decrease. However, it should be mentioned that it was much more difficult to discern the influence of the horizontal length of lens on I and i when properties of sandy clay loam were assigned to the lens (rather than sand), when a constant head boundary was assigned at the top of the sandy lens (rather than assuming a full reservoir), and for greater subsurface heterogeneity in soil hydraulic properties.

3.2.3. Stochastic heterogeneity

Although the above results demonstrate that the soil hydraulic properties of individual soil layers can be accurately determined during constant head infiltration experiments, the noted limitations indicate that it is unlikely to accurately determine the lateral extension of these layers/lenses under heterogeneous field conditions. The heterogeneous stochastic simulations discussed in Figs. 3 and 5 were therefore analyzed in terms of equivalent homogeneous profile values of K_s and α that were inversely fitted to I for each stochastic realization. Average values of K_s and α, and their 95% confidence intervals, were determined from 100 realizations using a given set of stochastic parameters. Fig. 10 presents average values of K_s as a function of the stochastic parameters σ (Fig. 10A with $X = 1$ and $Z = 0.1$), X (Fig. 10B with $\sigma = 1$ and $Z = 0.1$, and Fig. 10C with$\sigma = 1$ and $Z = 2$), and Z (Fig. 10D with $\sigma = 1$ and $X = 1$) and the K_s value of sandy loam from the HYDRUS (2D/3D) Soil catalog. The average values of $K_s$were found to be highly sensitive to different stochastic parameters and exhibited very narrow 95% confidence intervals. In particular, average values of K_s increase with σ and X, but decrease with Z. Similar to I in Figs. 3 and 5, this can be attributed to increasing amounts of high permeability lenses with greater lateral extensions with increasing σ and X, and isolated high permeability zones with increasing Z. The average K_s value for stochastic heterogeneous domains was always higher than the homogeneous domain (Fig. 12A). A highly heterogeneous ($\sigma = 1$) domain with many high and low permeable lateral lenses connected vertically via short highly permeable lenses (i.e., $X = 10$, $Z = 0.1$; $X = 10$, $Z = 2$; $X = 0.1$, Z = 0.1; and $X = 1$, $Z = 0.1$) had the highest average K_s value (Fig. 12A).

Fig. 11 presents average values of α as a function of the stochastic parameters σ (Fig. 11A with $X = 1$ and $Z = 0.1$), X (Fig. 11B with $\sigma = 1$ and $Z = 0.1$, and Fig. 11C with $\sigma = 1$ and $Z = 2$), and Z (Fig. 11D with $\sigma = 1$ and $X = 1$) and the α value of sandy loam from the HYDRUS (2D/3D) Soil catalog. Average values of α ranged between 2.44 and 8.46 m^{-1} and had a relatively large confidence interval (Fig. 12B) compared to the average values of K_s with a very tight confidence interval (Fig. 12A). Furthermore, a sensitivity analysis ofK_s and α were conducted where one of the parameters (i.e. either K_s or α) was kept as constant in each direct simulation and the cumulative infiltration volume was determined (Data is not shown). Average value of $K_s = 3.94 \times 10^{-3}$, 8.19×10^{-4} and 2.44×10^{-4} m min^{-1} and $\alpha = 8.46$, 7.5, and 2.44 m^{-1} were used (Fig. 12). The results from the sensitivity analysis demonstrated that the cumulative infiltration volume increases with increase in K_s and α values at a given condition. However, the observations from sensitivity analysis, Figs. 10–12 indicate that the average value of K_s plays a primary role and the value of α played a secondary role in determining the cumulative infiltration volume and long-term performance of a drywell. A large K_s value indicates the presence of a highly conductive soil that leads to the faster infiltration. Whereas, a large α value indicates a uniform and sharp wetting front and a small α value indicates a nonuniform and dispersed wetting front (Carsel and Parrish, 1988; Elrick et al., 1989; Rawls et al., 1982; van Genuchten et al., 1991). Additional numerical experiments are needed to understand this topic better, which was not further investigated in this study.

Fig. 13 shows a comparison of I simulated for a homogeneous sandy loam soil profile with K_s and α values obtained from the HYDRUS (2D/3D) Soil catalog ($K_s = 7.37 \times 10^{-4}$ m min^{-1} and $\alpha = 7.5\ m^{-1}$) (Table 1), inversely optimized average value of $K_s = 3.94 \times 10^{-3}$ m min^{-1} and$\alpha = 6.17\ m^{-1}$, Upper-Confidence-Interval values of $K_s = 3.68 \times 10^{-3}$ m min^{-1} and $\alpha = 5.40\ m^{-1}$, and Lower-Confidence-Interval values of $K_s = 4.20 \times 10^{-3}$ m min^{-1} and $\alpha = 6.94\ m^{-1}$ for the heterogeneous domain with the following stochastic parameters: $\sigma = 1$, $X = 10$, and $Z = 0.1$. Average values of K_s and I increased by 435% and 396% for the stochastic domain. Note that all these simulations were conducted for a homogeneous flow domain with a sandy loam soil for 5760 min (96 h) by keeping a constant head at the surface of the drywell.

Replacing the heterogeneous domain with an equivalent homogeneous domain as presented in this study can accurately predict long-term cumulative infiltration (96 h), which is relevant for the Low Impact Development Standard for drywells (LACDPW, 2014). Therefore, a detailed characterization of heterogeneity in soil hydraulic properties, which is very time consuming and expensive, may not be required when water quantity is the only criterion for evaluating drywell performance. This research demonstrates that falling or constant head drywell infiltration experiments can be used in conjunction with HYDRUS (2D/3D) numerical modeling to inversely estimate effective hydraulic properties for a heterogeneous drywell site that can be used to accurately assess its infiltration performance. A constant head experiment can accurately provide the average hydraulic properties of a drywell site. However, a constant head experiment may not account for hydraulic properties (position, lateral extension, and thickness of high permeable lenses) of sites presented in Fig. 2 that are highly relevant factors affecting the cumulative infiltration volume in a falling head experiment. The hydraulic properties determined using a falling head experiment may thus underestimate or overestimate the cumulative infiltration volume compared to the hydraulic properties obtained from a constant head experiment. Therefore, this research demonstrates that a constant head drywell infiltration experiment coupled with HYDRUS (2D/3D) inverse optimization of hydraulic parameters of each layer of a multi-layered soil system (Table 2 and Fig. 8) is the best method to accurately estimate the hydraulic property of a drywell site and to assess the long-term performance of a drywell.

4. Conclusions

The numerical modeling results presented in this study demonstrate the application of HYDRUS (2D/3D) in predicting the cumulative infiltration volume and in determining soil hydraulic properties adjacent to a drywell. In particular, numerical experiments were conducted to better understand the influence of deterministic and stochastic heterogeneity in soil hydraulic properties on drywell infiltration behavior. Results demonstrated that a highly permeable lens/layer at the bottom of a drywell can infiltrate water at a much faster rate than the same sized lens at the top of a drywell. Furthermore, the cumulative infiltration volume from a drywell increases with an increasing lateral extension and thickness of a high permeable lens. Similarly, the average cumulative infiltration volume from 100 stochastic realizations increased with increasing σ and lateral correlation length but decreased with an increasing vertical correlation length.

The result from direct and indirect numerical experiments provided

insight in developing field scale falling head and constant head experimental methods for drywell to determine the in-situ soil hydraulic properties of multiple soil layers and high permeable lenses to characterize drywell infiltration. Numerical experiments demonstrated that constant head experiments provide higher accuracy in inversely optimized hydraulic parameters than falling head experiments. However, inverse determination of soil hydraulic properties for individual soil lenses of varying lateral extensions may be impractical for highly heterogeneous systems. The hydraulic properties for stochastic experiments with heterogeneous soil distributions were therefore characterized in terms of an equivalent homogeneous soil profile. The average value of K_s from multiple stochastic realizations with the same parameter sets had the greatest influence and played a primary role on drywell cumulative infiltration. The α value showed a larger confidence interval and thus played a secondary role in the overall drywell performance. Similar to cumulative infiltration, the average value of K_s increased with σ and the lateral correlation length, but decreased with an increasing vertical correlation length.

The equivalent homogeneous hydraulic properties obtained from a heterogeneous domain can be used to estimate the infiltration from a drywell. However, the hydraulic properties obtained from a falling head experiment may over or underestimate the cumulative infiltration volume compared to the hydraulic properties obtained from a constant head experiment. Therefore, a constant head experiment for multi-layered soil system would be the best method to accurately determine the drywell site hydraulic property and its long-term performance. This research demonstrates that extensive soil characterization may not be necessary if water quantity is the only concern. However, if the drywell performance also needs to account for water quality, including the fate and transport of pathogenic microbial contaminants such as virus and/or bacteria, an accurate estimation of site heterogeneity is expected to be very important. Ongoing research in our lab is currently investigating this further.

Acknowledgments

Funding for this research was provided by the U.S. Environmental Protection Agency (US EPA) through an interagency agreement with the United States Department of Agriculture (EPA DW-012-92465401; ARS 60-2022-7-002). The views expressed in this article are those of the authors and do not necessarily represent the views or policies of the U.S. Environmental Protection Agency. Mention of commercial products does not constitute an endorsement.

References

Archer, N., Bonell, M., MacDonald, A., Coles, N., 2014. A constant head well permeameter formula comparison: its significance in the estimation of field-saturated hydraulic conductivity in heterogeneous shallow soils. Hydrol. Res. 45 (6), 788–805.

Bouwer, H., 2002. Artificial recharge of groundwater: hydrogeology and engineering. Hydrogeol. J. 10 (1), 121–142. https://doi.org/10.1007/s10040-001-0182-4.

Bouwer, H., Back, J.T., Oliver, J.M., 1999. Predicting infiltration and ground-water mounds for artificial recharge. J. Hydrol. Eng. 4 (4), 350–357. https://doi.org/10.1061/(ASCE)1084-0699(1999) 4:4(350).

Carsel, R.F., Parrish, R.S., 1988. Developing joint probability distributions of soil water retention characteristics. Water Resour. Res. 24 (5), 755–769.

Dillon, P., 2005. Future management of aquifer recharge. Hydrogeol. J. 13 (1), 313–316. https://doi.org/10.1007/s10040-004-0413-6.

Edwards, E.C., Harter, T., Fogg, G.E., Washburn, B., Hamad, H., 2016. Assessing the effectiveness of drywells as tools for stormwater management and aquifer recharge and their groundwater contamination potential. J. Hydrol. 539, 539–553. https://doi.org/10.1016/j.jhydrol.2016.05.059.

Elrick, D.E., Reynolds, W.D., Tan, K.A., 1989. Hydraulic conductivity measurements in the unsaturated zone using improved well analyses. Ground Water Monit. R 9 (3), 184–193. https://doi.org/10.1111/j.1745-6592.1989.tb01162.x.

Hammel, K., Roth, K., 1998. Approximation of asymptotic dispersivity of conservative solute in unsaturated heterogeneous media with steady-state flow. Water Resour. Res. 34 (4), 709–715. https://doi.org/10.1029/98WR00004.

Hodges, M.K.V., Orr, S.M., Potter, K.E., LeMaitre, T., 2012. Construction diagrams, geophysical logs, and lithologic descriptions for boreholes, Idaho National Laboratory, USGS 103, 105, 108, 131, 135, NRF-15, and NRF-16.

Jain, P., Powell, J., Townsend, T.G., Reinhart, D.R., 2006. Estimating the hydraulic conductivity of landfilled municipal solid waste using the borehole permeameter test. J. Environ. Eng. 132 (6), 645–652.

Kummu, M., Guillaume, J.H.A., De Moel, H., Eisner, S., Flörke, M., Porkka, M., Siebert, S., Veldkamp, T.I.E., Ward, P.J., 2016. The world's road to water scarcity: shortage and stress in the 20th century and pathways towards sustainability. Sci. Rep. 6, 38495. https://doi.org/10.1038/srep38495.

LACDPW, 2014. Low Impact Development. County of Los Angeles Department of Public Works Standards Manual (2014) 1-496.

Marquardt, D.W., 1963. An algorithm for least-squares estimation of nonlinear parameters. J. Soc. Ind. Appl. Math. 11 (2), 431–441. https://doi.org/10.1137/0111030.

Miller, E., Miller, R., 1956. Physical theory for capillary flow phenomena. J. Appl. Phys. 27 (4), 324–332. https://doi.org/10.1063/1.1722370.

Mualem, Y., 1976. A new model for predicting the hydraulic conductivity of unsaturated porous media. Water Resour. Res. 12 (3), 513–522. https://doi.org/10.1029/WR012i003p00513.

Philip, J., 1985. Approximate analysis of the borehole permeameter in unsaturated soil. Water Resour. Res. 21 (7), 1025–1033.

Postel, S.L., 2000. Entering an era of water scarcity: the challenges ahead. Ecol. Appl. 10 (4), 941–948. https://doi.org/10.2307/2641009.

Postel, S.L., Daily, G.C., Ehrlich, P.R., 1996. Human appropriation of renewable fresh water. Science 271 (5250), 785–788. https://doi.org/10.1126/science.271.5250.785.

Rassam, D., Šimůnek, J., Van Genuchten, M.T., 2003. Modeling variably saturated flow with HYDRUS-2D. ND Consult.

Rawls, W.J., Brakensiek, D., Saxtonn, K., 1982. Estimation of soil water properties. Trans. ASAE 25 (5), 1316–1320.

Reynolds, W., Elrick, D., 1985. In situ measurement of field-saturated hydraulic conductivity, sorptivity, and the [alpha]-parameter using the Guelph permeameter. Soil Sci. 140 (4), 292–302.

Rosegrant, M.W., Cai, X., Cline, S.A., 2002. World Water and food to 2025: dealing with scarcity. Int. Food Policy Res. Inst.

Roth, K., 1995. Steady state flow in an unsaturated, two-dimensional, macroscopically homogeneous miller-similar medium. Water Resour. Res. 31 (9), 2127–2140.

Roth, K., Hammel, K., 1996. Transport of conservative chemical through an unsaturated two-dimensional Miller-similar medium with steady-state flow. Water Resour. Res. 32 (6), 1653–1663. https://doi.org/10.1029/95WR00946.

Sasidharan, S., Bradford, S.A., Šimůnek, J., DeJong, B., Kraemer, S.R., 2018. Evaluating drywells for stormwater management and enhanced aquifer recharge. Adv. Water Resour. 116, 167–177. https://doi.org/10.1016/j.advwatres.2018.04.003.

Šejna, M., Šimůnek, J., van Genuchten, M.T., 2014. The HYDRUS Software Package for Simulating the Two- and Three-Dimensional Movement of Water, Heat, and Multiple Solutes in Variably-Saturated Porous Media, User Manual, Version 2.04. PC-Progress, Prague, Czech Republic. 1-307.

Shiklomanov, I.A., 2000. Appraisal and assessment of world water resources. Water Int. 25 (1), 11–32. https://doi.org/10.1080/02508060008686794.

Šimůnek, J., van Genuchten, M. Th., and Šejna, M., 2011. The HYDRUS Software Package for Simulating Two- and Three-Dimensional Movement of Water, Heat, and Multiple Solutes in Variably-Saturated Porous Media, Technical Manual, Version 2.0, PC Progress, Prague, Czech Republic, pp. 258.

Šimůnek, J., Šejna, M., van Genuchten, M.T., 2018. New features of version 3 of the HYDRUS (2D/3D) computer software package. J. Hydrol. Hydromech. 66 (2), 133–142. https://doi.org/10.1515/johh-2017-0050.

Šimůnek, J., van Genuchten, M.T., Šejna, M., 2016. Recent developments and applications of the HYDRUS computer software packages. Vadose Zone J. 15 (7), 25. https://doi.org/10.2136/vzj2016.04.0033.

Tseng, P.H., Jury, W.A., 1994. Comparison of transfer function and deterministic modeling of area-averaged solute transport in a heterogeneous field. Water Resour. Res. 30 (7), 2051–2063. https://doi.org/10.1029/94WR00752.

van Genuchten, M.T., 1980. A closed-form equation for predicting the hydraulic conductivity of unsaturated soils. Soil Sci. Soc. Am. J. 44 (5), 892–898.

van Genuchten, M.T., Leij, F., Yates, S., 1991. The RETC code for quantifying the hydraulic functions of unsaturated soils. IAG-DW12933934, U.S. Salinity Laboratory, U. S. Department of Agriculture, Agricultural Research Service, Riverside, California.

Vereecken, H., Kasteel, R., Vanderborght, J., Harter, T., 2007. Upscaling hydraulic properties and soil water flow processes in heterogeneous soils. Vadose Zone J. 6 (1), 1–28. https://doi.org/10.2136/vzj2006.0055.

Watt, E., Marsalek, J., 2013. Critical review of the evolution of the design storm event concept. Can. J. Civ. Eng. 40 (2), 105–113. https://doi.org/10.1139/cjce-2011-0594.

Weeks, E.P., 1978. Field determination of vertical permeability to air in the unsaturated zone. Department of the Interior, Geological Survey.

Xiang, J., Chen, L., 1993. Users' manual for LAYERK.VI-a code to evaluate the tield hydraulic conductivity layered media in unsaturated for zone. Bureau of Economic Geology, The University of Texas at Austin.

Xiang, J., Scanlon, B., Mullican, W., Chen, L., Goldsmith, R., 1997. A multistep constant-head borehole test to determine field saturated hydraulic conductivity of layered soils. Adv. Water Resour. 20 (1), 45–57. https://doi.org/10.1016/S0309-1708(96)00017-6.